ACS PHYSICAL CHEMISTRY Au
AN OPEN ACCESS JOURNAL OF THE AMERICAN CHEMICAL SOCIETY

pubs.acs.org/physchemau

Article

Structural Water Molecules Confined in Soft and Hard Nanocavities as Bright Color Emitters

Jiafeng Zhou, Taiqun Yang, Bo Peng, Bingqian Shan, Meng Ding, and Kun Zhang*

Cite This: *ACS Phys. Chem Au* 2022, 2, 47−58

Read Online

ACCESS | Metrics & More | Article Recommendations | Supporting Information

ABSTRACT: Molecules confined in the nanocavity and nanointerface exhibit rich, unique physicochemical properties, e.g., the chromophore in the β-barrel can of green fluorescent protein (GFP) exhibits tunable bright colors. However, the physical origin of their photoluminescence (PL) emission remains elusive. To mimic the microenvironment of the GFP protein scaffold at the molecule level, two groups of nanocavities were created by molecule self-assembly using organic chromophores and by organic functionalization of mesoporous silica, respectively. We provide strong evidence that structural water molecules confined in these nanocavities are color emitters with a universal formula of $\{X^+\cdot(OH^-\cdot H_2O)\cdot(H_2O)_{n-1}\}$, in which X is hydrated protons (H_3O^+) or protonated amino (NH_3^+) groups as an anchoring point, and that the efficiency of PL is strongly dependent on the stability of the main emitter centers of the structural hydrated hydroxide complex ($OH^-\cdot H_2O$), which is a key intermediate to mediate electron transfer dominated by proton transfer at confined nanospace. Further controlled experiments and combined characterizations by time-resolved steady-state and ultrafast transient optical spectroscopy unveil an unusual multichannel radiative and/or nonradiative mechanism dominated by quantum transient states with a distinctive character of topological excitation. The finding of this work underscores the pivotal role of structurally bound H_2O in regulating the PL efficiency of aggregation-induced emission luminogens and GFP.

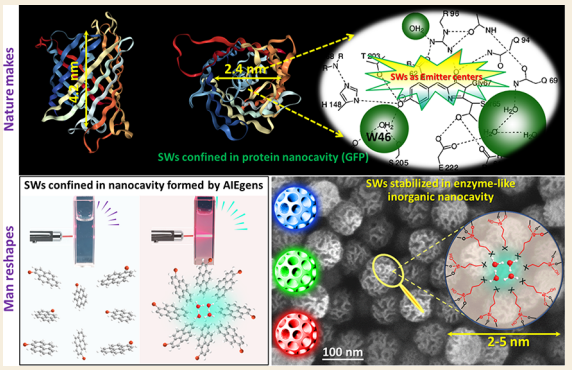

KEYWORDS: *green fluorescent protein (GFP), aggregation-induced emission, nanocavity, structural water molecules (SWs), hydrated hydroxide complex, quantum transient states, topological excitation*

INTRODUCTION

Under ambient conditions, most surfaces are covered by water molecules. However, the influence of the adsorption of water molecules on the interfacial state at nanoscale interfaces was seriously overlooked in both chemistry and biology. A huge amount of experimental evidence proves that the first contact layer of water is not comprised of pure water but instead of a mixture of water and hydroxyl molecules (or hydrous hydroxide complexes).[1−4] It forms because it affords the optimal balance of H-bonding within the overlayer and bonding to the surface,[5] which has now been observed on several transition metal oxides,[6] metal surfaces,[7] and even in biology systems, such as green fluorescent protein (GFP).[8,9] Intrinsically, free water molecules are colorless liquid. The pioneered ab initio path-integral molecular dynamics (PIMD) simulations exhibit that, at a confined nanocavity and interface, due to many-body nuclear quantum effects (MBNQEs), the overlapping of p orbitals of O atoms in water clusters could produce some exotic quantum states, whose electron localization excitation is extremely susceptible to the structural inhomogeneity and local environments.[10−16] But water clusters as color emitters were not proved experimentally.[17,18]

The aggregation-induced emission (AIE) effect was first proposed by Tang and his co-workers in 2001, which now has been intensively investigated.[19,20] To restrict the intramolecular motions (RIMs) in solution, the design of AIE luminogens (AIEgens) with a special chemical structure is necessary in the earlier reported results, e.g., diphenyl-1-pyrenylphosphine (**DPPP**) with unique AIE rotors.[21−23] However, just by an AIE mechanism, many abnormal photoluminescence (PL) properties of simple AIEgens with nonconjugated structures cannot be easily understood, such as tetraphenylethane (**TPE**) and 1,2-diphenylethane (s-**DPE**),[24−26] and even currently used 1-bromopyrene (**BP**). It is importantly noted that the nature of AIE is indeed a solvent-driven molecular self-assembly process, in which the poor solvent water is commonly used as a mixed solvent.

Received: August 23, 2021
Revised: September 24, 2021
Accepted: September 24, 2021
Published: October 14, 2021

https://doi.org/10.1021/acsphyschemau.1c00020
ACS Phys. Chem Au 2022, 2, 47−58

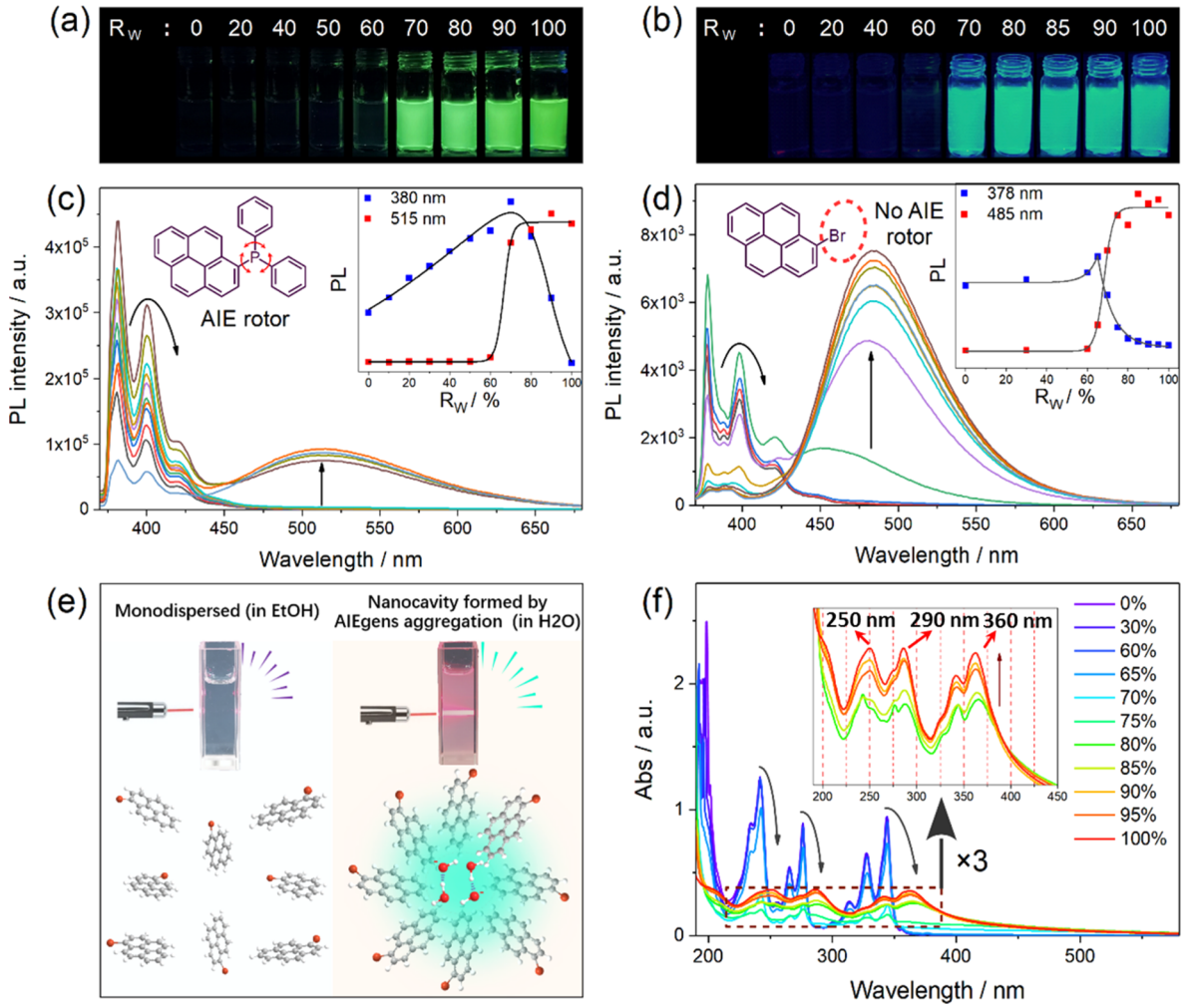

Figure 1. (a,b) Photographs and (c,d) fluorescence spectra of **DPPP** (a,c) and 1-bromopyrene (b,d) in mixed solvents with different volume fractions R_w (R_w = Vol_w/Vol_{e+w}, the subscripts w and e represent water and ethanol, respectively). Inset shows the relationship between the luminescence intensity and R_w. (e) Proposed mechanism for water-induced AIE phenomenon. (f) Ultraviolet−visible (UV−vis) absorption spectra of 1-bromopyrene (**BP**) in mixed solvents with different R_w. All of the spectra were recorded immediately after the sample added into the mixture solvents; the concentration of **DPPP** and **BP** was 10 and 100 μmol/L, respectively. Noting that all spectra acquisition needs to be accomplished at a very short time (within 6 s), since **DPPP** is very sensitive to the UV light.

Considering the possible quantum effect of hydrogen-bonded water molecules in confined space, there is a hidden possibility that water clusters in the nanocavity formed by AIEgens are the true luminous center,[27] instead of the aggregate itself. This also inspires us to propose a question: what is the true emitter of GFP, a self-catalyzed formed organic chromophore or structural water molecules in the proximity of an organic chromophore?[28−31] Even though, in some cases, the poor solvent water was not used, if we carefully checked the purity of used organic solvents, the adsorption of trace of water into the system (even for solid AIEgens) cannot be completely avoided during the preparation and PL measurement of AIEgens under open moisture environments. Herein, our research provides direct evidence that SWs confined in AIEgens and a silica matrix functionalized with simple amino ($-NH_2$) or carboxyl (−COOH) groups could act as an emitter center to tune the PL emission with bright colors and demonstrates that its PL efficacy, including colors, quantum yield, and lifetimes are strongly dependent on the rate of proton transfer in the delicately balanced H-bond networks. The conceptual of confined structural water molecules (SWs) as a bright emitter provides a new insight into understanding the physical origin of PL of nonconventional chromophores in a confined nanospace.

RESULTS AND DISCUSSION

Nanocavity Formed by Aggregation of Typical AIEgens of Diphenyl-1-pyrenylphosphine (DPPP) and Tetraphenylethylene (TPE) and Classical Organic Chromophores (1-Bromopyrene, BP) for SW Hosting

Two typical AIEgens of **DPPP** and **TPE** derivatives are deliberately selected to create the nanocavity by their self-assembly (Figures S1−S4). As previously reported, the as-synthesized **DPPP** aggregate exhibits strong solvophilicity-dependent photoluminescence emission features due to the AIE effect,[23] as shown in Figure 1a,c. When dissolved in ethanol solution, the **DPPP** molecule only exhibits three fingerprint emission peaks ($\lambda_{max} \approx$ 380, 400, and 420 nm) within the range of about 370−450 nm, which correspond to the characteristic emission peaks of a single pyrene molecule (Figure 1c,d). When **DPPP** was dispersed into the mixed solution of water and ethanol, with an increase of the volume

https://doi.org/10.1021/acsphyschemau.1c00020
ACS Phys. Chem Au 2022, 2, 47−58

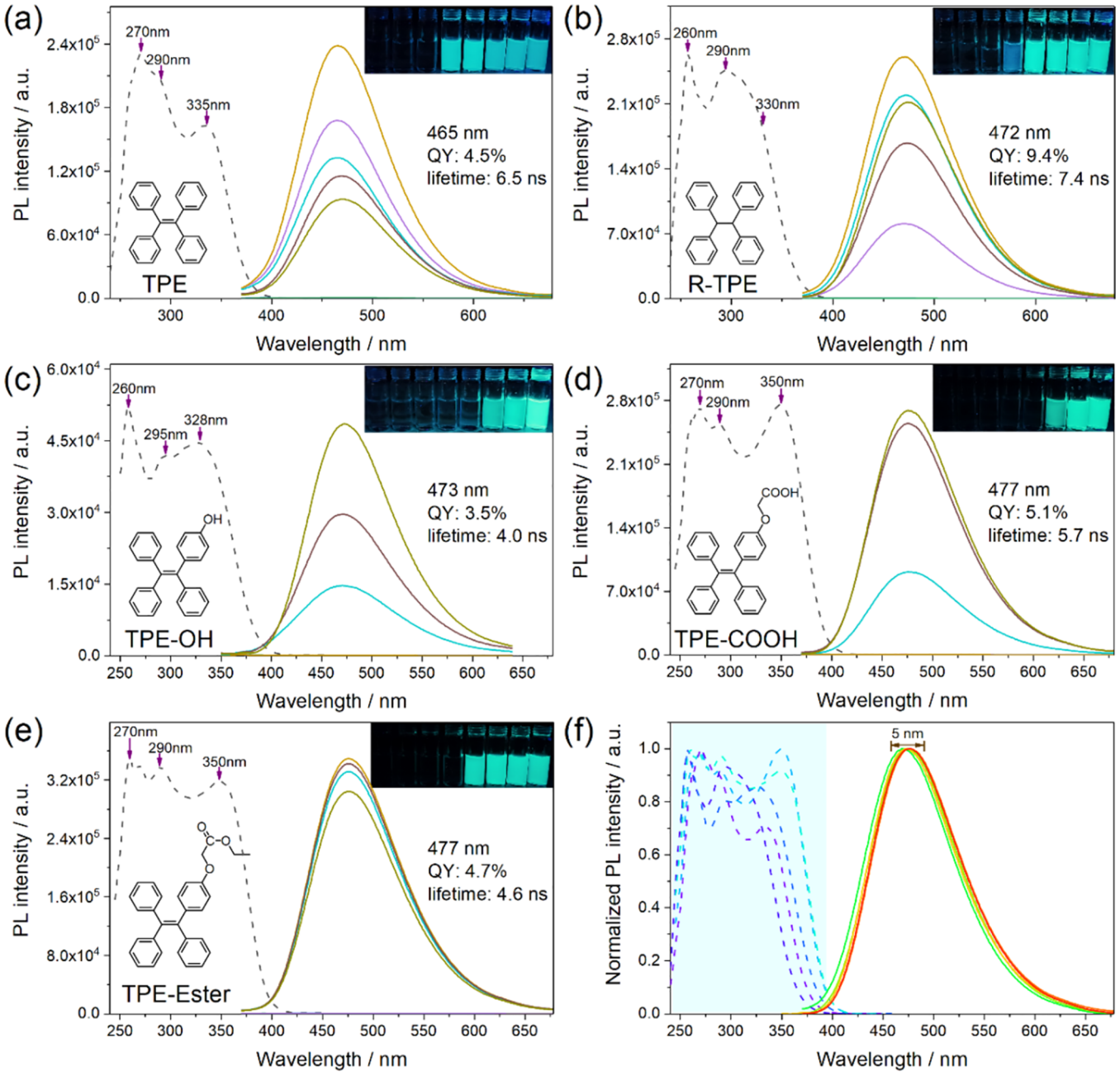

Figure 2. (a–e) Fluorescence spectra of five kinds of **TPE** derivatives in mixed solvents with different volume fractions (R_w: 0, 20, 40, 60, 70, 80, 90, 100%). Inset shows the corresponding digital photos under UV light. (f) Normalized fluorescence spectra of five kinds of TPE derivatives in water (R_w = 100%). The concentration of **TPE** derivatives was 100 μmol/L.

fraction of water in the solvent (R_w = Vol_w/Vol_{e+w}, the subscripts w and e represent water and ethanol, respectively), the PL of **DPPP** molecules gradually intensified when R_w was increased to 70% and then suddenly dropped sharply due to the ACQ effect. When R_w exceeded a critical value ($R_w \geq$ 70%), a new broad bright emission emerged at ∼515 nm with an fwhm around 100 nm intensified with the further increase of R_w, which is generally attributed to AIE enhancement (Figure 1e, right, an obvious Tyndall effect indicates the formation of aggregates).

With the increase of R_w (≤60%), the adsorption spectra (Figure S5a) show that three inherent adsorptions of **DPPP** at 241, 280, and 365 nm are gradually increased and that, when $R_w \geq$ 70%, all the adsorption bands show a red-shift of ∼10 nm, identical to that of **BP** molecules (Figure 1f). What is the nature of the three adsorption bands at 285, 345, and 375 nm? Are they newly formed or just the red-shift of **DPPP** by the AIE effect? Meanwhile, the excitation spectra detected at emissions of 380 and 400 nm exhibit completely different evolution trends (Figure S5b,c): at $R_w \leq$ 60%, the intensity of excitation of **DPPP** first increases and gets the maximum value at R_w = 70% and then decreases due to the ACQ effect, but the three excitation bands do not show any shifts, which precludes the possibility of an absorption red-shift caused by the aggregation of **DPPP** molecules. When detected at an emission of 515 nm (Figure S5d), if the $R_w \leq$ 60%, the excitation spectra are silent; only when $R_w \geq$ 70%, three new broad excitation bands at 285, 345, and 375 nm are observed, and to our

https://doi.org/10.1021/acsphyschemau.1c00020
ACS Phys. Chem Au 2022, 2, 47–58

surprise, the main excitation band to the emission of 515 nm is located at 285 nm (Figure S5d). Generally, according to the AIE mechanism, $\pi-\pi$ stacking by space interactions leads to the red-shift emission (515 nm), which must accompany a red-shift of the excitation band. Our observation confirms an abnormal PL behavior, i.e., long wavelength emission triggered by short wavelength excitation, which was only observed for SWs confined in the subnanopores of LTA zeolites.[32] Thus, we assigned the new formed adsorption bands at 241, 280, and 365 nm to the feature adsorption of SWs. In addition, if we closely examine the inherent absorptions of **DPPP**, their inherent adsorption bands as a shoulder of newly formed three absorption bands of SWs can be easily distinguished at 241, 280, and 365 nm (Figure S5a), answering the shoulder emissions of **DPPP** even with $R_w \geq 70\%$ at 400 nm (Figures 1c and S5b,c).

To our big surprises, similar absorption, excitation, and emission spectra were also observed for 1-bromopyrene (**BP**) molecules (Figures 1d,f and S6), which is the conventional chromophore herein used as a precursor for the synthesis of **DPPP** AIEgens (Scheme S1 and Figure S1).[33] Thus, we confirmed that the propeller-like rotor structure was not indispensable for enhanced PL emission, implying a new emission mechanism, which is different from the well-accepted AIE mechanism. Note that both **DPPP** and **BP** aggregates in the mixed solvent exhibit similar emission properties, including a few percent emission quantum yield (QY) and a several nanosecond lifetime (Figure S7 and Table S1). The only difference of the **DPPP** AIEgen and **BP** in the emission spectra is the blue-shift of the emission band from 515 to 485 nm. As is well-known, **BP** is usually regarded as a concentration-quenching dye instead of an AIEgen, which is supported by the observation of emission spectrum (Figure 1d): with the increase of aggregation, the inherent PL emissions ($\lambda_{max} \approx 380$, 400, and 420 nm) of a single **BP** molecule were quenched due to ACQ, but a new emission band at 485 nm was observed, and its intensity was intensified, displaying the typical AIE behaviors.

Generally, with more densely packed aggregates triggered by the solvent effect with different volume fractions R_w, larger red-shift emission should be observed in both the conjugated electron delocalization model and nonconjugated electron space interaction model. However, the absorption and emission bands of both **DPPP** and **BP** molecules did not show any red-shifts (Figures 1c,d,f, S5, and S8). Very interestingly, if we carefully look at the details of the absorption spectrum of BP solution (Figure 1f, inset), when R_w exceeds a critical value ($R_w \geq 70\%$), three adsorption bands at 250, 290, and 360 nm are readily distinguished, concomitantly accompanying the PL emission at ∼485 nm. It is importantly noted that these typical adsorption bands are all observed for **DPPP**, **BP**, and **TPE** molecules with completely different chemical structures (Figure 2a−e). This cannot be simply explained by the AIE mechanism, which also differs from the physical mechanism of the local excitation of conventional organic chromophores.

In addition, if the PL emission of AIEgens is coming from the aggregate itself, the absorption and emission wavelength of AIEgens with varied functional groups should be changed. However, completely different **TPE** derivatives exhibit identical PL emission at ∼470 nm with identical multiple excitation bands in a range of 250−370 nm and a similar fluorescence lifetime of ∼5 ns (Figure 2 and Schemes S2−S4, Figures S2−S4 and S9, and Table S2). To our big surprise, the completely nonconjugated **R-TPE** shows a long wavelength emission (472 vs 465 nm) with long lifetime (7.4 vs 6.5 ns) and quantum yield (9.4 vs 4.5%), compared to TPE. Interestingly, the excitation spectrum is almost the same with three excitation bands at 260, 290, and 330 nm, which cannot be attributed to the adsorption of **TPE** and **R-TPE** themselves, since they have completely different molecular structures (Figure 2a,b). In addition, we note that even though **TPE** derivatives and **BP** have totally different chemical structures and conjugated structures, these two molecules at a critical R_w value of ∼60% show an identical PL emission at ∼480 nm (Figures 1d and Figure 2). We think it is not a simple coincidence, probably suggesting a new mechanism of PL emission of AIEgens. There is an overlooked fact that the nanocavity formed by water−AIEgens−ethanol ternary system is an ideal platform to host SWs as PL emitters, since all the hydrophobic organic chromophores at a critical value of R_w exhibit the presence of a pre-Ouzo structure, i.e., the formation of milk-like microemulsions (Figures 1e, S10, and S11).[34,35]

The dosing experiment of inorganic salts with varied hydration capacity and the isotope experiments of water tested this possibility of SWs as emitter centers. When various salts were introduced, the wavelength of fluorescence emission was not shifted, but the emission intensity increased, suggesting the increased stability of the emitter center of SWs (Figure S12a,b). It is importantly noted that, when we discuss the influence of the cation and anion effect of inorganic salts on PL properties, the counteranion and countercation of inorganic salts are fixed to be nitrate (Figure S12a) and sodium (Figure S12b), respectively. Since the aggregate of AIEgens is electrically neutral, the aggregation behavior will not be dramatically influenced when a low concentration of inorganic salts was introduced. Considering the proposed chemical structure of the emitter center as $\{X^+ \cdot (OH^- \cdot H_2O) \cdot (H_2O)_{n-1}\}$, the increase of PL with the introduction of inorganic salts should be attributed to the stabilization of emitters by removal of weakly adsorbed water molecules $(H_2O)_{n-1}$ around the hydrous hydroxide complex $(OH^- \cdot H_2O)$, because fast proton transfer in the H-bond network fluctuates the p orbital overlapping of O atoms. The surrounding water molecules were abstracted by salts, which blocks the proton shuttling in the hydrous hydroxide complex. The isotope tracing experiments of water molecules further prove the important role of proton transfer on PL emission. The dosing of D_2O with heavier deuterium shows the strongest PL emission due to slower diffusion rate, compared to $H_2{}^{18}O$ and H_2O (Figure S12c).[36] Thus, we tentatively assigned SWs confined in the nanocavity as emitters, completely differing from that of a conventional AIE mechanism, i.e., an aggregate itself.

There is direct evidence that a hydrous hydroxide complex as an emitter comes from the bright-colored DMSO solution with the introduction of a trace amount of NaOH in the absence of AIEgens, since both DMSO and NaOH molecules are silent in absorption and PL emission. Only upon the introduction of NaOH solution (1 M) does the inherent nonfluorescent DMSO exhibit PL emission at ∼505 nm (Figure 3), identical to that of currently used AIEgens, such as **DPPP**, **TPE**, and **BP** (Figures 1 and 2), and with the increase of NaOH concentration, its intensity was gradually intensified. Thus, we can preclude the possibility that the introduction of impurities of organic chromopheres in DMSO solvent acts as emitters, since we used the same bottle of DMSO as solvent.

https://doi.org/10.1021/acsphyschemau.1c00020
ACS Phys. Chem Au 2022, 2, 47−58

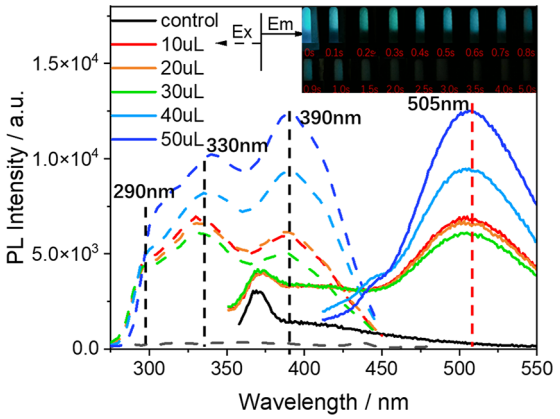

Figure 3. Excitation (dashed line) and emission (solid line) spectra of sodium hydroxide solution (1 M) in DMSO free of AIEgens (inset, emission photographs of sodium hydroxide solution with ultralong lifetimes up to 5 s at liquid nitrogen temperature).

Three readily distinguished excitation bands at 290, 330, and 390 nm in alkaline solution of DMSO were also observed in AIEgens (Figures 3 and 2, dashed line), implying their common PL origin. The PL emission dominated by these excitation bands has the typical characteristics of a $\pi-\pi^*$ transition, which is obvious due to the p orbital overlapping of O atoms in a hydrous hydroxide ($H_2O{\cdot}OH^-$) complex though space interactions.[10,14] Very interestingly, at liquid nitrogen temperature, DMSO solution in the presence of NaOH displays ultralong PL lifetimes up to 5 s (Figure 3, inset), which was never reported before. The ultralong lifetime observation of DMSO solution is attributed to the stable orbital overlapping between O atoms where low temperature slows down the transfer or shuttling of protons in the H-bonding networks of a hydrous hydroxide complex.[14] Thus, we provide direct evidence that the origin of AIEgens is coming from the structural water molecules (SWs).

Mimicking the Tertiary Structure of Native GFPs to Fabricate an Organic Function-Modified Mesoporous Silica Nanocavity for Bright-Colored Structural Water Molecules

In fact, SWs not only confined in the soft nanocavity of AIEgens but also in the hard nanocavity of mesopoorus silica emit tunable bright colors. Using mesoporous silica nanospheres (MSNs) with spherical pores of ~3 nm as an inorganic matrix,[35,37] reminiscent of the size and shape of the β-can of 4.2 by 2.4 nm folded by 11 β-strands of GFP (Figure S13), the fluorescent MSNs (FMSNs) without the incorporation of chromophores were designed to show the central role of gusted SWs for the PL emission. To fabricate the binding or adsorption sites of SWs in confined mesopores and mimic the microenvironment of GFP, the silica was functionalized by customer-tailored organic functions with nonconjugated structures, such as simple amino ($-NH_2$) and carboxyl ($-COOH$) groups. Similar amino acid R96 and E222 residues in the nanocavity of GFP were reported to play a pivotal role to tune PL.[8]

It is important to note that both individual amino and succinic functional groups are nonluminescent in solution. With a commonly used surface grafting technique,[38] the amino and carboxyl groups were successfully covalently tethered onto the surface of mesopores using aminopropyl triethoxysilane (or N-(2-aminoethyl)-3-amino-propyltrimethoxysilane) and 3-(triethoxysilyl) propylsuccinic anhydride as a coupling agent, respectively (Figures 4a,b and S14). Note that, under the atmosphere, the succinic functional groups react rapidly with moisture/water to the carboxyl ($-COOH$) groups. For clarity, the succinic functional group is denoted as carboxyl group. Very interestingly, MSNs emit very strong PL luminescence with tunable colors from blue to red, and the absorption and emission bands strongly depend on the grafted organic functions (Figure 4c,d). The amino-functionalized MSNs showed a striking blue-light fluorescence emission at ~430 nm, and their excitation and emission spectra completely matched, implying a nonconventional molecule local excitation (Figure 4c), since the chromophores are absent in FMSNs. Meanwhile, the carboxyl-functionalized MSNs exhibited a remarkable red-color emission at ca. 615 nm (Figure 4d). Time-resolved PL spectra showed that both samples have short lifetimes of several ns and moderate quantum yield (~1.0%), similar to that of GFP.[8,30]

Most recently, Tang's group and some of us proposed the concept of "nonconjugated organic functions clustering triggers AIE" by space interactions to elucidate the physical origin of PL emission of noble metal NCs, sugars, polymers, etc.[20] However, the water evacuation experiment of luminescent H_2N--@Meso-silica at low temperature precludes the amino- and carboxyl-group-clustering-induced AIE enhancement: if water was extracted, the PL intensity at ~450 nm was almost quenched (Figure 5); however, if the sample was exposed to the moisture atmosphere, the original PL was gradually recovered. Thus, we definitively confirmed that the PL of FMSNs is coming from the trapped water molecules in nanopores, in the form of structural water moleculess (SWs), instead of the clustering of organic functions. It should be mentioned that, herein, SWs are not a simple dimer of water molecule formed by hydrogen bonding, but a hydrous hydroxide complex with a π bonding characteristic formed by the spatial overlap of p orbitals of two O atoms in SWs. Intrinsically, free water molecules are colorless liquid. However, due to the many-body nuclear quantum effects (MBNQEs) of O atoms in the confined nanocavity of MSNs, some new quantum states emerge through the space overlapping of the p orbitals of O atoms in SWs,[39,40] whose intense and multiple adsorption bands have $\pi-\pi^*$ transition characteristics. Obviously, the energy level and lifetimes of these quantum states were determined together by the overlapping degree of p orbitals and the rate of proton transfer (or shuttling) in the H-bond network. The following designed diagnostic experiments to fluctuate the H-bond network, including surface hydrophobicity control, proton trapping by ultralow temperature and pH, and the salt effect, further evidence the rationality of SWs as emitter centers, which have a structure of $\{X^+{\cdot}(OH^-{\cdot}H_2O){\cdot}(H_2O)_{n-1}\}$.

Surface hydrophobicity significantly affects the fabrication of the H-bond network and the rate of proton transfer. As expected, with the increase of hydrophobicity of NH_2-FMSNs, the excitation bands exhibit a red-shift from 350 to 475 nm, and concomitantly, the emission band red-shifts from blue color (ca. 430 nm) to green color (ca. 530 nm) (Figure 4e). It is clear that higher surface hydrophobicity breaks the network of H-bonds, which blocks the proton transfer, maximizing the overlap between the p orbitals of oxygen atoms in the hydrate hydroxide complex ($OH^-{\cdot}H_2O$). Consequently, the maximum overlapping of p orbitals lowers the energy level of new formed quantum states, resulting in the

https://doi.org/10.1021/acsphyschemau.1c00020
ACS Phys. Chem Au 2022, 2, 47−58

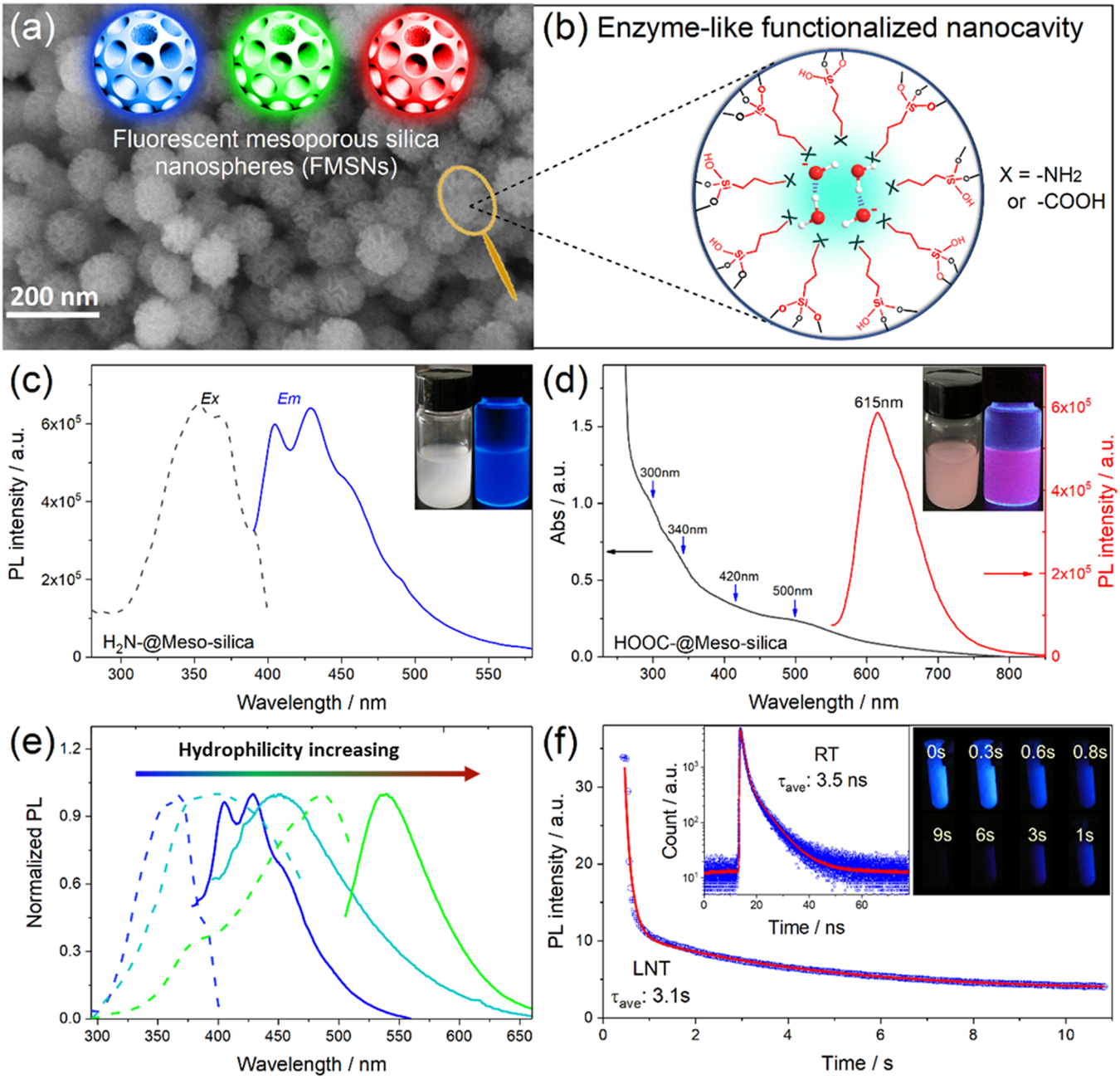

Figure 4. (a) Scanning electron microscopy (SEM) of as-synthesized fluorescent mesoporous silica nanoparticles (FMSNs). Inset shows the cartoon of FMSNs with different emission wavelengths by surface modification under different conditions. (b) The formation of SWs in an amino- and carbonyl-group-functionalized enzyme-like nanocavity. (c) Excitation and emission spectra of aminopropyl-functionalized FMSNs. (d) Absorption and emission spectra of propylsuccinic-functionalized FMSNs. Note that, in the atmosphere, the succinic functional groups react rapidly with moisture/water to the carboxyl (−COOH) groups. Thus, for clarity and simplicity, in the cartoon, succinic groups were marked as carboxyl (−COOH) groups. (e) Emission wavelength regulation of FMSNs by controlling the hydrophobicity of the nanopores. Normalized excitation (dashed) and emission (solid) spectra of amino-functionalized DMSN (NH_2−FMSNs) with hydrophobic treatment. The hydrophobic functional groups (trimethyl chlorosilane: TMCS) were gradually decreased from 4 equiv (blue) to 1 equiv (green), and the emission wavelength was red-shifted from ∼430 to ∼538 nm. (f) Time-resolved luminescence decay profiles of NH_2−FMSNs at room temperature (RT) and liquid nitrogen temperature (LNT). Inset shows the naked-eye-visible long afterglow emission of NH_2−FMSNs at LNT.

red-shift PL emissions. At this point, it is importantly noted that higher surface hydrophobicity (larger density of trimethylsilane groups) means larger spatial isolations between neighboring propylamino groups,[41,42] which precludes the "clustering triggered AIE" mechanism to PL emission of unconjugated organic functions by space interactions.[20] Very similar PL-emission-enhanced behavior in GFP was also observed, when surface hydrophobicity was increased by an irreversible photoinduced oxidative decarboxylation surrounding the chromophore.[43] Thus, just by simple surface hydrophobicity treatment, the color-tunable FMSNs could be readily prepared, much easier than GFP variants by genetically encodable mutation.

An ultralow temperature experiment at liquid nitrogen temperature (77 K) further evidences the pivotal role of proton transfer on PL (Figure 4f). When the FMSNs were

https://doi.org/10.1021/acsphyschemau.1c00020
ACS Phys. Chem Au 2022, 2, 47−58

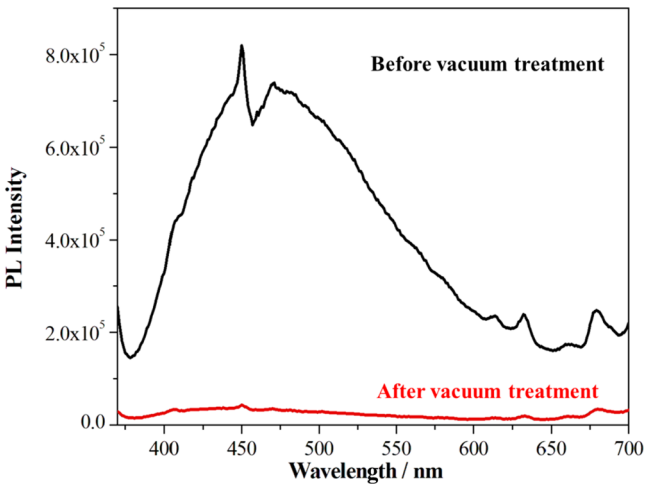

Figure 5. Evolution of PL emission intensity of amino-functionalized FMSNs at ca. 450 nm by vacuum dehydration treatment.

cooled down to liquid nitrogen temperature (77 K), an unprecedented ultralong quantum lifetime up to 10 s was observed with an 8 orders of magnitude increase, compared to ~3.5 ns at room temperature (Figure 4f). The increase of quantum lifetime is due to the slowing down of proton shuttling in the nanocavity at low temperature, which stabilized the dynamics of excited states. Our early reported electron paramagnetic resonance (EPR) results showed that the fast switching of hydroxide (OH^-) to water in the mesopores on the ns scale was almost suspended at the liquid nitrogen temperature (LNT) due to the blocking of proton transfer.[38] If the structure of $\{NH_3^+\cdot(H_3O_2)^-\cdot(H_2O)_{n-1}\}$ emitter center is right, pH and the salt effect will also be the main factors to determine the PL efficiency of emitter centers.

Our acid titration experiments further prove the rationality of the emitter structure of hydrous hydroxide complex, since the intensity and position of PL emission are extremely sensitive to the variation of pH value (Figure 6a). With a decrease of pH value from 8.45 to 2.15, the PL intensity of FMSNs was first slightly decreased, then raised again and passed though the maximum at pH of 3.2, and finally decreased again. Concomitantly, a blue-shift of PL emission was observed from ~425 to ~380 nm (Figure 6a). Because the pK_a of the proprylamino group is ~10.60, the parent amino-group-functionalized MSNs show a weak alkaline (pH ≈ 8.50). With the decrease of pH, part of the amino groups is protonated to amino positive cations (NH_3^+), which could be a prefect anchoring site to hydrate the hydroxide complex in the form of $\{NH_3^+\cdot(OH^-\cdot H_2O)\}$. If more acid was introduced, the structure of the hydrate hydroxide complex will be broken due to the acid−base neutralization reaction. This answers the evolution of the PL intensity with the pH (Figure 6a). Meanwhile, more acid introduces more protons shuttle between the emitter centers, which perturbs the overlapping of p orbitals between O atoms. Consequently, it leads to the blue-shift of PL emission of FMSNs (Figure 6a). It is worth to note that the protonation of amino groups is obviously disadvantageous to the clustering of functional groups due to the electrostatic repulsions. In addition, the protonation will diminish the number of unpaired electrons (or lone electron

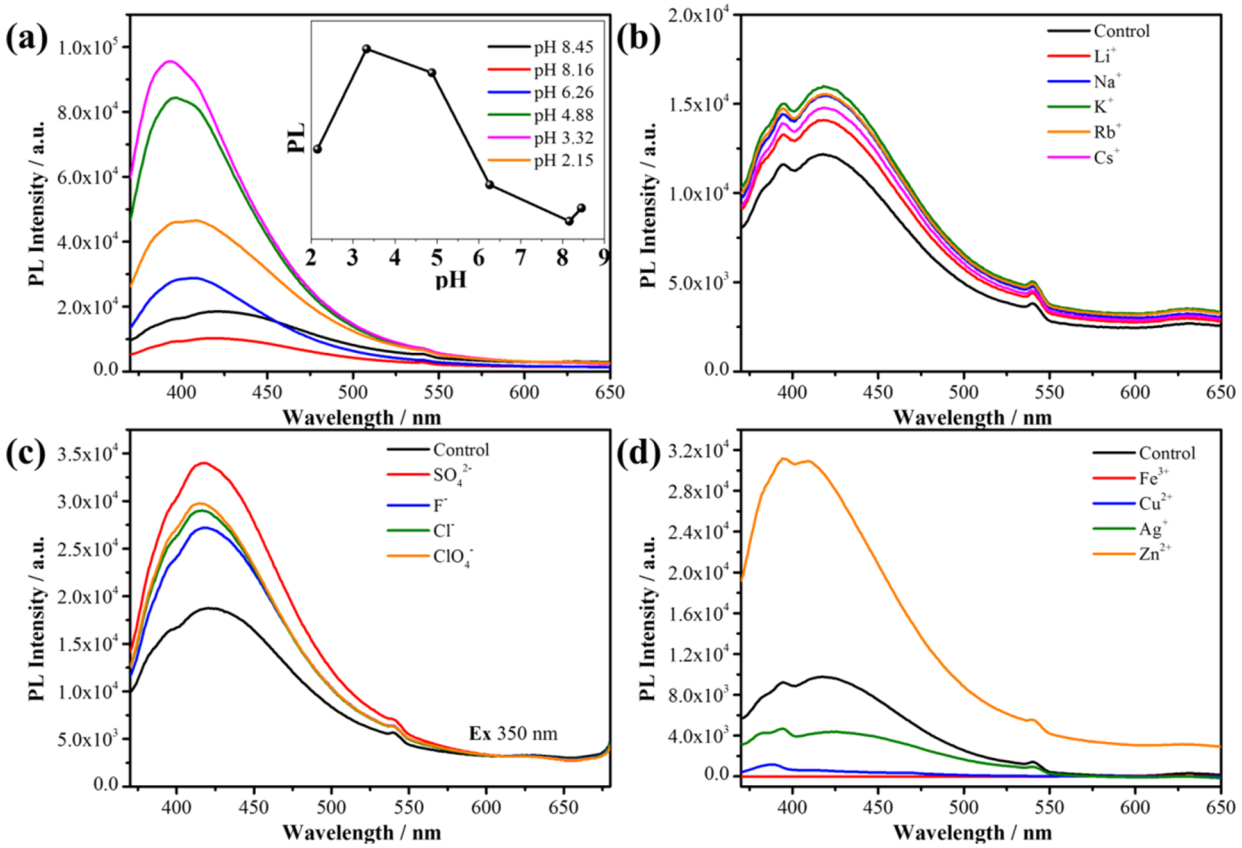

Figure 6. (a) Emission spectra of NH_2−FMSNs in water solution with different pH values. Emission spectra of NH_2−FMSNs with different cations (b,d) and anions (c). The concentration of ions was 5 mmol/L. All spectra are obtained with 350 nm excitation.

https://doi.org/10.1021/acsphyschemau.1c00020
ACS Phys. Chem Au 2022, 2, 47−58

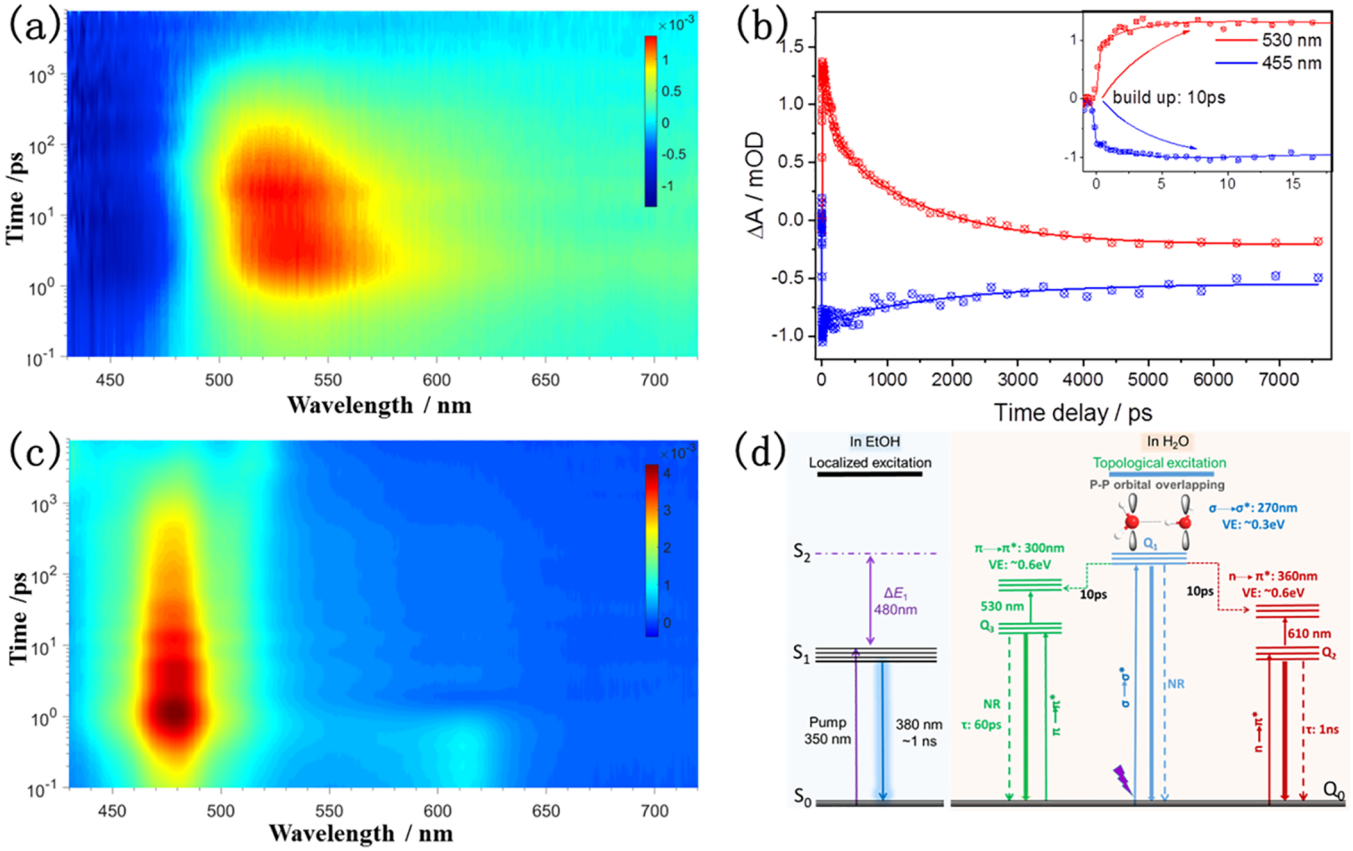

Figure 7. Contour representation of the multidimensional time-resolved transient absorption (TA) data for **BP** in H_2O (a) and EtOH (c). (b) Selected decay traces at 455 and 530 nm and corresponding fitting of **BP** in water solution; the fitting results are summarized in Table S4. (d) Energy levels and relaxation pathway of SWs under different solvent conditions (Q_n means the multiple quantum transient states, which are produced by the dynamic p orbital overlapping of paired oxygen in the hydrated hydroxide complexes. Dashed downward arrows refer to the nonradiative decay, and straight upward and downward arrows refer, respectively, to the optical absorption and fluorescence transitions with denoted colors.).

pairs) on N atoms. Both factors are not good for PL emission enhancement by a clustering-induced AIE effect.[20] Thus, the assignment of $\{NH_3^+\cdot(OH^-\cdot H_2O)\cdot(H_2O)_{n-1}\}$ as an emitter center is reasonable, since water is the only rest molecule in the nanopores.

The salt effect of varied inorganic electrolytes further proves that, in the emitter center, there are two types of water molecules: normal water molecules with weak H-bonding interactions, i.e, $(H_2O)_{n-1}$, and a very stabilized hydroxide complex $(OH^-\cdot H_2O)$ with semichemical covalent bonds. Because of the characteristic of $(H_2O)_{n-1}$ with weak H-bond interactions, these water molecules can be readily abstracted by the hydration of cations and anions of general inorganic salts, such as sodium salts (NaX, X = SO_4^{2-}, F^-, Cl^-, and ClO_4^-) and chloride alkali metals (MCl, M = Li, Na, K, Rb, and Cs). Thus, upon the addition of these salts, the PL intensity of FMSNs is increased due to the breaking of the H-bond network, which blocks the proton transfer (Figure 6b,c). However, the position of the emission bands almost does not show any shifts (Figure 6b,c). However, when transition metal cations, i.e., $M_x(NO_3)_y$ (M = Zn, Fe, Cu, and Ag) are introduced, except Zn^{2+}, the PL of FMSNs was dramatically diminished probably due to the strong competing coordination interaction of the hydroxide group in $OH^-\cdot H_2O$ anionic complexes with metal cations (Figure 6 d), suggesting the chemical bond of $OH^-\cdot H_2O$ has the strength of the dative (coordinative) bond. The enhancement effect of Zn^{2+} addition on the PL of FMSNs is beyond our understanding (Figure 6d) but suggests a super stabilization of Zn^{2+} on the emitter center. The completely same PL enhancement effect of Zn^{2+} was also observed in GFP,[33] suggesting a similar PL emission mechanism with FMSNs. Based on this discovery, we suppose that the emitter center of GFP is not an organic chromophore of *p*-hydroxybenzylidene−imidazolidinone (HBDI−OH), which is formed by internal cyclization of Ser65, Tyr66, and Gly67. Instead, the structural water molecules (SWs) confined in in the center of the β-barrel of GFP are the true color emitter, where the anionic HBDI−O^- chromophore may play a hydroxyl role to form the {(HBDI−O^-W46) (≡R} emitter center (in the formula, W46 means H-boned water with HBDI, and ≡R means the conserved amino acid residues in the proximity of the chromophore (Figure S13).[8] This also answers that the PL properties of GFP are extremely sensitive to the surrounding environment of chromophores, in particular, such as the architecture of the β-barrel, a delicate change of amino acid residues, and the pH value.

Taken together, we proposed that the SWs in the nanocavity are present in the form of $\{NH_3^+\cdot(OH^-\cdot H_2O)\cdot(H_2O)_{n-1}\}$, where protonated amine is anchoring sites by a singly hydrated hydroxide complex $(OH^-\cdot H_2O)$, which is surrounded by water molecules with normal H-bonds. Note that owing to the quantum fluctuation of the H nucleus (proton transfer or shuttle), the formed multiple quantum states have a transient feature, which was captured by femtosecond time-resolved

https://doi.org/10.1021/acsphyschemau.1c00020
ACS Phys. Chem Au 2022, 2, 47−58

transient absorption (TA) spectra (Figure 7).[32] The overlapping degree and the rate of proton transfer between two O atoms in the hydrous hydroxide complex determine the PL properties, including the colors, quantum yield, and lifetimes.

Kinetics of Quantum Transient States of SWs in the Confined Nanocavity

To understand the dynamics of quantum transient states of SWs in the confined nanocavity, the femtosecond time-resolved transient absorption (TA) spectra for **BP** AIEgens in solvent of H_2O and EtOH with an excitation of 350 nm was performed (Figure 7a,c). By simultaneously monitoring the decay of the excited-state absorption (ESA) and recovery of the stimulated emission (SE), the fs-TA enables dynamic interplay and branching ratios of the states during the nonradiative decay to be quantified. As expected, a transient absorption band of **BP** molecules centered at 475 nm in ethanol was observed, which is assigned to the excited-state absorptions (ESA) of the **BP** molecule itself (Figure 7c). When **BP** molecules were dispersed into water solution, two broad signals peaking at 455 and 530 nm were captured (Figure 7a), which were assigned to the stimulated emission (SE) due to the PL emission at 485 nm (Figure 1b) and the excited-state absorption of SWs in the aggregated nanocavity, respectively. Meanwhile, the SE at ∼485 nm displays recovery with a time profile completely mirroring the decay of ESAs at ∼530 nm in the 10 ps scale, providing clear evidence for electron transfer between the quantum transient states dominated by H-bonding interactions in several tens ps of lifetimes (Figure 7b, inset). Global analysis of the decay profiles of **BP** in water at all wavelengths (Figure S15 and Table S4) observed complex dynamics requiring a description by multiexponentials containing at least three components with time constants in the early picosecond (τ_1 = ∼3.0 ps), close to dozens of picoseconds (τ_2 = ∼60 ps), and about a nanosecond (τ_3 = ∼1.0 ns) time scale. The fractional contribution (α%) of each component (Table S4) varies according to the emission wavelength with those of the two slower components featuring greater contributions at longer wavelength.

The fs-TA suggests a scenario of deactivation involving the energy delocalized excitation producing an ensemble of quantum transient states (Q_n) with mutually different polarizations that decay via multiple channels (Figure 7d, right in light-yellow background): The first quantum transient state (Q1) may arise due to the direct $\sigma-\sigma^*$ dipole transition of O−H bond of water molecules involved in the photoabsorption, corresponding to the higher energy adsorptions and excitations of steady optical absorptions (Figure 4c,d); Q_2 and Q_3 bands are attributed to the $\pi-\pi^*$ and/or $n-\pi^*$ fluorescence transition dipoles due to the dynamic p orbital overlapping of paired oxygen, exhibiting much longer decay times with the charge transfer character. The observed ultrafast electron excitation transfer is very similar to dynamic switching of interface bonding between the chemisorption and physisorption dominated by interfacial vibration decay kinetics recently reported by Borodin et al.[44] Meanwhile, the close analysis of the weighting amplitudes derived from the multiexponential TA decays at the varied emission wavelengths showed that these quantum transient states (Q_n) are correlated with each other (Figure S15 and Table S4, answering that the signal of TA almost covers the entire visible wavelengths with two distinguished peaks at 530 and 610 nm (Figures 7a and S15a). The behavior of the complex dynamics of **BP** aggregates suggests the formation of exotic quantum transient states, completely differing from the localized excitation of a conventional chromophore molecule (like a single **BP** molecule, Figure 7d, left in light-blue background), and we call it topological excitation. First of all, topology is a mathematical concept, that is, "invariance in change", which is borrowed by physics to explain the motion state of basic particles and even some strange quantum properties. In the current description of structural water molecules $\{OH^-\cdot H_2O\}$ as emitters, we can image that, at an uncertain ultrafast transient moment, the outmost p orbitals of two oxygen atoms not only maintain their own orbital characteristics (invariance) but also have the characteristics of spatial delocalization (variability), which provide a variety of radiationless electron transfer channels (reaction channels for catalysis) to bright color emissions, which is completely consistent with the characterization results of an ultrafast transient absorption spectrum.[32] This also answers the nature of the interfacial state or bonding of heterogeneous catalysis between reactants and/or support (in particular, the metal nanoscale interface).[45−51]

The origin of the topological excitation is probably coming from the dynamic combinations of p orbitals of two oxygen atoms in hydrous hydroxide complexes ($OH^-\cdot H_2O$) though space interactions. The nature of these exotic excitonic states has a dynamic bonding feature, and its stability and PL properties strongly depend on the H-bond interactions of hydrous hydroxide complexes in the confined nanocavity, such as OH dissociation of water and proton shuttling, which probably explains the anomalous ultralong quantum lifetime of AIEgens and FMSNs up to 10 s at liquid nitrogen temperature. This also explains the recently observed anomalously low dielectric constant of water under extreme confinement.[52,53] Thus, the main deactivation pathways for SWs confined in the nanocavity can be depicted as such: this involves the extremely rapid electron excitation energy transition from the initial excitation localized states (Q_1) and the subsequent 10 ps decay of the Q_1 exciton that simultaneously bifurcates leading to the long-living Q_2 and Q_3 states with $\pi-\pi^*$ and/or $n-\pi^*$ fluorescence transition dipoles, respectively, at the same time formation by excitation energy transfer; these states then revert, respectively, into background state with the different rates but comparably high efficiencies, which altogether account for the vast majority of the entire deactivation and PL emissions (Figure 6d, right in a light-yellow background). Very recently, the same deactivation pathway for proteins and G-quadruplexes was reported, but their PL origin was unfortunately assigned to the intrinsic interbase electronic couplings and the delocalization of excitation.[54−57]

CONCLUSIONS

Based on the solid experimental evidence, we first demonstrated that structural water molecules (SWs) in the confined nanocavity are true emitter centers, whose structure has a universal formula of $\{X^+\cdot(OH^-\cdot H_2O)(H_2O)_{n-1}\}$ and adsorbed on the X sites by electrostatic interaction. Its PL efficiency is extremely sensitive to the microenvironment of emitter centers like GFP, which is dominated by proton transfer dynamics. The PL origin of SWs was attributed to the many-body quantum electron correlations in the confined nanocavity where an ensemble of quantum transient states was produced due to the dynamic p orbital overlapping of paired oxygen atoms in the hydrated hydroxide complexes though space interactions. The proposed model not only elucidates the

https://doi.org/10.1021/acsphyschemau.1c00020
ACS Phys. Chem Au 2022, 2, 47−58

nature of AIE effect in chemistry but also answers the photophysics and photochemistry of GFP in a biology system.[58] Most importantly, considering the universality of water adsorption at many interfaces, the PL mechanism of all the low dimensional quantum nanodots, including the metal nanoclusters (NCs),[59−61] carbon or graphene oxide (GO) dots,[62] MOFs,[63] metal cation exchanged zeolites,[64,65] supermolecules,[66−71] nontraditional chromophores without conjugated structures,[69,72] small-size green-emitting push−pull fluorophores,[73,74] perovskites,[75,76] and even semiconductors,[77] should be revisited. In additions, the discovery of SWs with varied stability and multiple intermediate states at the nanoscale interface probably answers the promoting role of surface hydroxyl groups and alkali metal ions on the electrocatalytic reaction of water splitting (HER, OER, and ORR),[78] the reduction of 4-nitrophenol (4-NP) and CO_2,[49−51] and the water−gas shift reaction (WGSR)[45,46,48] by providing alternative channels for concerted proton and electron transfer.

■ ASSOCIATED CONTENT

Supporting Information

The Supporting Information is available free of charge at https://pubs.acs.org/doi/10.1021/acsphyschemau.1c00020.

Synthesis and characterization of the organic molecules related with AIEgens and MSNs; absorption, excitation, and time-resolved luminescence decay profiles spectra of organic molecules related with AIEgens and MSNs (PDF)

■ AUTHOR INFORMATION

Corresponding Author

Kun Zhang − *Shanghai Key Laboratory of Green Chemistry and Chemical Processes, College of Chemistry and Molecular Engineering, East China Normal University, Shanghai 200062, China; Laboratoire de chimie, Ecole Normale Supérieure de Lyon, Institut de Chimie de Lyon, Université de Lyon, 69364 Lyon cedex 07, France; Shandong Provincial Key Laboratory of Chemical Energy Storage and Novel Cell Technology, School of Chemistry and Chemical Engineering, Liaocheng University, Liaocheng 252059 Shandong, P. R. China;* orcid.org/0000-0001-8418-1424; Email: kzhang@chem.ecnu.edu.cn

Authors

Jiafeng Zhou − *Shanghai Key Laboratory of Green Chemistry and Chemical Processes, College of Chemistry and Molecular Engineering, East China Normal University, Shanghai 200062, China*

Taiqun Yang − *Shanghai Key Laboratory of Green Chemistry and Chemical Processes, College of Chemistry and Molecular Engineering, East China Normal University, Shanghai 200062, China*

Bo Peng − *Shanghai Key Laboratory of Green Chemistry and Chemical Processes, College of Chemistry and Molecular Engineering, East China Normal University, Shanghai 200062, China*

Bingqian Shan − *Shanghai Key Laboratory of Green Chemistry and Chemical Processes, College of Chemistry and Molecular Engineering, East China Normal University, Shanghai 200062, China*

Meng Ding − *Shanghai Key Laboratory of Green Chemistry and Chemical Processes, College of Chemistry and Molecular Engineering, East China Normal University, Shanghai 200062, China*

Complete contact information is available at: https://pubs.acs.org/10.1021/acsphyschemau.1c00020

Author Contributions

K.Z. conceived and directed the project. K.Z. independently proposed the concept of structural water molecules (SWs) as an emitter center by topological excitation and used this model to elucidate the PL origin of green fluorescent proteins (GFPs). T.Q.Y., B.P., and J.F.Z. equally contributed to this research. J.F.Z. synthesized AIEgens and their derivatives. B.P. and M.D. prepared and characterized the FMSNs. T.Q.Y. performed the PL and TA measurements. B.Q.S. performed the SEM and TEM measurements. K.Z. designed the figures and wrote the manuscript with the help of T.Q.Y. All authors have read and agreed to the published version of the manuscript.

Notes

The authors declare no competing financial interest.

■ ACKNOWLEDGMENTS

This research was funded by the NSFC (22172051, 21872053, and 21573074), the Science and Technology Commission of Shanghai Municipality (19520711400), the CAS key laboratory of Low-Coal Conversion Science & Engineering (KLLCCSE-201702), and the JORISS program. K.Z. thanks ENS de Lyon for a temporary position as an invited professor in France. We also appreciate Prof. Shuanhu Gao for their great help in the synthesis of AIEgens at East China Normal University. This paper is dedicated to my two mentors, Prof. Ming-Yuan He at ECNU and Prof. Laurent Bonneviot at ENS-Lyon, on the occasion of their 80th and 65th birthdays, respectively.

■ REFERENCES

(1) Meier, M.; et al. Water agglomerates on Fe3O4 (001). *Proc. Natl. Acad. Sci. U. S. A.* **2018**, *115*, E5642−E5650.

(2) Coudert, F.-X. Water Adsorption in Soft and Heterogeneous Nanopores. *Acc. Chem. Res.* **2020**, *53*, 1342−1350.

(3) Mouhat, F.; Coudert, F.-X.; Bocquet, M.-L. Structure and chemistry of graphene oxide in liquid water from first principles. *Nat. Commun.* **2020**, *11*, 1566.

(4) Hu, X.-D.; Yang, T.; Shan, B.; Peng, B.; Zhang, K. Topological excitation of singly hydrated hydroxide complex in confined sub-nanospace for bright color emission and heterogeneous catalysis. *ChemRxiv* 2020.

(5) Li, X.-Z.; Probert, M. I.; Alavi, A.; Michaelides, A. Quantum nature of the proton in water-hydroxyl overlayers on metal surfaces. *Phys. Rev. Lett.* **2010**, *104*, No. 066102.

(6) Yuan, W.; et al. Visualizing H2O molecules reacting at TiO2 active sites with transmission electron microscopy. *Science* **2020**, *367*, 428−430.

(7) Kumagai, T.; et al. Symmetric hydrogen bond in a water-hydroxyl complex on Cu (110). *Phys. Rev. B: Condens. Matter Mater. Phys.* **2010**, *81*, No. 045402.

(8) Craggs, T. D. Green fluorescent protein: structure, folding and chromophore maturation. *Chem. Soc. Rev.* **2009**, *38*, 2865−2875.

(9) Scholes, G. D.; et al. Using coherence to enhance function in chemical and biophysical systems. *Nature* **2017**, *543*, 647−656.

(10) Tuckerman, M. E.; Marx, D.; Klein, M. L.; Parrinello, M. On the quantum nature of the shared proton in hydrogen bonds. *Science* **1997**, *275*, 817−820.

(11) Meng, X.; et al. Direct visualization of concerted proton tunnelling in a water nanocluster. *Nat. Phys.* **2015**, *11*, 235−239.
(12) Guo, J.; et al. Nuclear quantum effects of hydrogen bonds probed by tip-enhanced inelastic electron tunneling. *Science* **2016**, *352*, 321−325.
(13) Richardson, J. O.; et al. Concerted hydrogen-bond breaking by quantum tunneling in the water hexamer prism. *Science* **2016**, *351*, 1310−1313.
(14) Guo, J.; Li, X.-Z.; Peng, J.; Wang, E.-G.; Jiang, Y. Atomic-scale investigation of nuclear quantum effects of surface water: Experiments and theory. *Prog. Surf. Sci.* **2017**, *92*, 203−239.
(15) Peng, J.; et al. The effect of hydration number on the interfacial transport of sodium ions. *Nature* **2018**, *557*, 701−705.
(16) Coudert, F.-X.; Boutin, A.; Fuchs, A. H. Open questions on water confined in nanoporous materials. *Communications Chemistry* **2021**, *4*, 106.
(17) Ewles, J. Water as an activator of luminescence. *Nature* **1930**, *125*, 706−707.
(18) Przibram, K. *Nature* **1958**, *182*, 520−520.
(19) Luo, J.; et al. Aggregation-induced emission of 1-methyl-1, 2, 3, 4, 5-pentaphenylsilole. *Chem. Commun.* **2001**, 1740−1741.
(20) Zhang, H.; et al. Clusterization-triggered emission: Uncommon luminescence from common materials. *Mater. Today* **2020**, *32*, 275−292.
(21) Kong, Y. J.; et al. Photoresponsive Propeller-like Chiral AIE Copper (I) Clusters. *Angew. Chem.* **2020**, *132*, 5374−5378.
(22) Wu, X.; et al. Exploiting racemism enhanced organic room-temperature phosphorescence to demonstrate Wallach's rule in the lighting chiral chromophores. *Nat. Commun.* **2020**, *11*, 2145.
(23) Xing, C.; et al. Diphenyl-1-pyrenylphosphine: photo-triggered AIE/ACQ transition with remarkable third-order nonlinear optical signal change. *Chem. Commun.* **2020**, *56*, 4220−4223.
(24) Li, Q.; Li, Z. The strong light-emission materials in the aggregated state: what happens from a single molecule to the collective group. *Advanced science* **2017**, *4*, 1600484.
(25) Zhang, H.; et al. Why do simple molecules with "isolated" phenyl rings emit visible light? *J. Am. Chem. Soc.* **2017**, *139*, 16264−16272.
(26) Zhang, H.; et al. Visualization and manipulation of molecular motion in the solid state through photoinduced clusteroluminescence. *J. Phys. Chem. Lett.* **2019**, *10*, 7077−7085.
(27) Vaitheeswaran, S.; Yin, H.; Rasaiah, J. C.; Hummer, G. Water clusters in nonpolar cavities. *Proc. Natl. Acad. Sci. U. S. A.* **2004**, *101*, 17002−17005.
(28) Tsien, R. Y. The green fluorescent protein. *Annu. Rev. Biochem.* **1998**, *67*, 509−544.
(29) Dong, J.; Solntsev, K. M.; Tolbert, L. M. Activation and tuning of green fluorescent protein chromophore emission by alkyl substituent-mediated crystal packing. *J. Am. Chem. Soc.* **2009**, *131*, 662−670.
(30) Zimmer, M. GFP: from jellyfish to the Nobel prize and beyond. *Chem. Soc. Rev.* **2009**, *38*, 2823−2832.
(31) Tou, S.-L.; et al. Aggregation-induced emission of GFP-like chromophores via exclusion of solvent−solute hydrogen bonding. *Chem. Commun.* **2014**, *50*, 620−622.
(32) Yang, T.; et al. Caged structural water molecules emit tunable brighter colors by topological excitation. *Nanoscale* **2021**, *13*, 15058−15066.
(33) Baird, G. S.; Zacharias, D. A.; Tsien, R. Y. Circular permutation and receptor insertion within green fluorescent proteins. *Proc. Natl. Acad. Sci. U. S. A.* **1999**, *96*, 11241−11246.
(34) Zemb, T. N.; et al. How to explain microemulsions formed by solvent mixtures without conventional surfactants. *Proc. Natl. Acad. Sci. U. S. A.* **2016**, *113*, 4260−4265.
(35) Hao, P.; Peng, B.; Shan, B.-Q.; Yang, T.-Q.; Zhang, K. Comprehensive understanding of the synthesis and formation mechanism of dendritic mesoporous silica nanospheres. *Nanoscale Advances* **2020**, *2*, 1792−1810.
(36) Berger, A.; Ciardi, G.; Sidler, D.; Hamm, P.; Shalit, A. Impact of nuclear quantum effects on the structural inhomogeneity of liquid water. *Proc. Natl. Acad. Sci. U. S. A.* **2019**, *116*, 2458−2463.
(37) Zhang, K.; et al. Facile large-scale synthesis of monodisperse mesoporous silica nanospheres with tunable pore structure. *J. Am. Chem. Soc.* **2013**, *135*, 2427−2430.
(38) Zhang, K.; et al. Mononuclear−Dinuclear Equilibrium of Grafted Copper Complexes Confined in the Nanochannels of MCM-41 Silica. *Chem. - Eur. J.* **2011**, *17*, 14258.
(39) Hoffmann, R. Interaction of orbitals through space and through bonds. *Acc. Chem. Res.* **1971**, *4*, 1−9.
(40) Yang, T.; et al. P band intermediate state (PBIS) tailors photoluminescence emission at confined nanoscale interface. *Communications Chemistry* **2019**, *2*, 132.
(41) Abry, S.; et al. Design of grafted copper complex in mesoporous silica in defined coordination, hydrophobicity and confinement states. *New J. Chem.* **2009**, *33*, 484−496.
(42) Zhang, K.; Albela, B.; He, M.-Y.; Wang, Y.; Bonneviot, L. Tetramethyl ammonium as masking agent for molecular stencil patterning in the confined space of the nano-channels of 2D hexagonal-templated porous silicas. *Phys. Chem. Chem. Phys.* **2009**, *11*, 2912−2921.
(43) Sample, V.; Newman, R. H.; Zhang, J. The structure and function of fluorescent proteins. *Chem. Soc. Rev.* **2009**, *38*, 2852−2864.
(44) Borodin, D.; et al. Following the microscopic pathway to adsorption through chemisorption and physisorption wells. *Science* **2020**, *369*, 1461−1465.
(45) Fu, Q.; Saltsburg, H.; Flytzani-Stephanopoulos, M. Active nonmetallic Au and Pt species on ceria-based water-gas shift catalysts. *Science* **2003**, *301*, 935−938.
(46) Yang, M.; et al. Catalytically active Au-O(OH)x- species stabilized by alkali ions on zeolites and mesoporous oxides. *Science* **2014**, *346*, 1498−1501.
(47) Medford, A. J.; et al. From the Sabatier principle to a predictive theory of transition-metal heterogeneous catalysis. *J. Catal.* **2015**, *328*, 36−42.
(48) Yang, M.; et al. A Common Single-Site Pt(II)−O(OH)x− Species Stabilized by Sodium on "Active" and "Inert" Supports Catalyzes the Water-Gas Shift Reaction. *J. Am. Chem. Soc.* **2015**, *137*, 3470−3473.
(49) Hu, X.-D.; Shan, B.-Q.; Tao, R.; Yang, T.-Q.; Zhang, K. Interfacial Hydroxyl Promotes the Reduction of 4-Nitrophenol by Ag-based Catalysts Confined in Dendritic Mesoporous Silica Nanospheres. *J. Phys. Chem. C* **2021**, *125*, 2446−2453.
(50) Shan, B.-Q.; Zhou, J.-F.; Ding, M.; Hu, X.-D.; Zhang, K. Surface electronic states mediate concerted electron and proton transfer at metal nanoscale interfaces for catalytic hydride reduction of − NO2 to − NH2. *Phys. Chem. Chem. Phys.* **2021**, *23*, 12950−12957.
(51) Tao, R.; et al. Surface Molecule Manipulated Pt/TiO2 Catalysts for Selective Hydrogenation of Cinnamaldehyde. *J. Phys. Chem. C* **2021**, *125*, 13304−13312.
(52) Fumagalli, L.; et al. Anomalously low dielectric constant of confined water. *Science* **2018**, *360*, 1339−1342.
(53) Geim, A. K. Exploring Two-Dimensional Empty Space. *Nano Lett.* **2021**, *21* (15), 6356−6358.
(54) Onidas, D.; Markovitsi, D.; Marguet, S.; Sharonov, A.; Gustavsson, T. Fluorescence properties of DNA nucleosides and nucleotides: a refined steady-state and femtosecond investigation. *J. Phys. Chem. B* **2002**, *106*, 11367−11374.
(55) Crespo-Hernández, C. E.; Cohen, B.; Kohler, B. Base stacking controls excited-state dynamics in A· T DNA. *Nature* **2005**, *436*, 1141−1144.
(56) Hua, Y.; Changenet-Barret, P.; Gustavsson, T.; Markovitsi, D. The effect of size on the optical properties of guanine nanostructures: a femtosecond to nanosecond study. *Phys. Chem. Chem. Phys.* **2013**, *15*, 7396−7402.
(57) Ma, C.; Chan, R. C.-T.; Chan, C. T.-L.; Wong, A. K.-W.; Kwok, W.-M. Real-time Monitoring Excitation Dynamics of Human

https://doi.org/10.1021/acsphyschemau.1c00020
ACS Phys. Chem Au 2022, 2, 47−58

Telomeric Guanine Quadruplexes: Effect of Folding Topology, Metal Cation, and Confinement by Nanocavity Water Pool. *J. Phys. Chem. Lett.* **2019**, *10*, 7577−7585.
(58) Romei, M. G.; Lin, C.-Y.; Mathews, I. I.; Boxer, S. G. Electrostatic control of photoisomerization pathways in proteins. *Science* **2020**, *367*, 76−79.
(59) Yang, T.; et al. Interfacial clustering-triggered fluorescence−phosphorescence dual solvoluminescence of metal nanoclusters. *J. Phys. Chem. Lett.* **2017**, *8*, 3980−3985.
(60) Yang, T.-Q.; et al. Origin of the photoluminescence of metal nanoclusters: from metal-centered emission to ligand-centered emission. *Nanomaterials* **2020**, *10*, 261.
(61) Peng, B.; et al. Physical origin of dual-emission of Au−Ag bimetallic nanoclusters. *Front. Chem.* **2021**, *9*, 756993.
(62) Baker, S. N.; Baker, G. A. Luminescent carbon nanodots: emergent nanolights. *Angew. Chem., Int. Ed.* **2010**, *49*, 6726−6744.
(63) Hu, Z.; Deibert, B. J.; Li, J. Luminescent metal−organic frameworks for chemical sensing and explosive detection. *Chem. Soc. Rev.* **2014**, *43*, 5815−5840.
(64) Coutino-Gonzalez, E.; et al. Silver Clusters in Zeolites: From Self-Assembly to Ground-Breaking Luminescent Properties. *Acc. Chem. Res.* **2017**, *50*, 2353−2361.
(65) Grandjean, D.; et al. Origin of the bright photoluminescence of few-atom silver clusters confined in LTA zeolites. *Science* **2018**, *361*, 686−690.
(66) Yan, X.; Cook, T. R.; Wang, P.; Huang, F.; Stang, P. J. Highly emissive platinum (II) metallacages. *Nat. Chem.* **2015**, *7*, 342−348.
(67) Datta, S.; Saha, M. L.; Stang, P. J. Hierarchical assemblies of supramolecular coordination complexes. *Acc. Chem. Res.* **2018**, *51*, 2047−2063.
(68) Zhou, Z.; et al. Understanding the effects of coordination and self-assembly on an emissive phenothiazine. *J. Am. Chem. Soc.* **2019**, *141*, 3717−3722.
(69) Wang, J.; Huang, Z.; Ma, X.; Tian, H. Visible-Light-Excited Room-Temperature Phosphorescence in Water by Cucurbit [8] uril-Mediated Supramolecular Assembly. *Angew. Chem., Int. Ed.* **2020**, *59*, 9928−9933.
(70) Wei, P.; et al. New Wine in Old Bottles: Prolonging Room-Temperature Phosphorescence of Crown Ethers by Supramolecular Interactions. *Angew. Chem., Int. Ed.* **2020**, *59*, 9293−9298.
(71) Wu, H.; et al. Ring-in-ring (s) complexes exhibiting tunable multicolor photoluminescence. *J. Am. Chem. Soc.* **2020**, *142*, 16849−16860.
(72) Zhou, Q.; et al. Clustering-triggered emission of nonconjugated polyacrylonitrile. *Small* **2016**, *12*, 6586−6592.
(73) Demeter, A.; et al. Dual fluorescence and fast intramolecular charge transfer with 4-(diisopropylamino) benzonitrile in alkane solvents. *Chem. Phys. Lett.* **2000**, *323*, 351−360.
(74) Kang, R.; et al. Discovery of a size-record breaking green-emissive fluorophore: small, smaller. *HINA. Chemical Science* **2021**, *12*, 1392−1397.
(75) Faheem, M. B.; et al. All-Inorganic Perovskite Solar Cells: Energetics, Key Challenges, and Strategies toward Commercialization. *ACS Energy Letters* **2020**, *5*, 290−320.
(76) Fan, Q.; et al. Lead-Free Halide Perovskite Nanocrystals: Crystal Structures, Synthesis, Stabilities, and Optical Properties. *Angew. Chem., Int. Ed.* **2020**, *59*, 1030−1046.
(77) Boles, M. A.; Ling, D.; Hyeon, T.; Talapin, D. V. The surface science of nanocrystals. *Nat. Mater.* **2016**, *15*, 141−153.
(78) Hong, W. T.; et al. Toward the rational design of non-precious transition metal oxides for oxygen electrocatalysis. *Energy Environ. Sci.* **2015**, *8*, 1404−1427.

https://doi.org/10.1021/acsphyschemau.1c00020
ACS Phys. Chem Au 2022, 2, 47−58